Limnol. Oceanogr., 49(1), 2004, 76–85

Observations of particle capture on a cylindrical collector: Implications for particle accumulation and removal in aquatic systems

Molly R. Palmer, Heidi M. Nepf,[1] and *Thomas J. R. Pettersson*
Ralph M. Parsons Laboratory, Department of Civil and Environmental Engineering, Massachusetts Institute of Technology, Cambridge, Massachusetts 02139

Josef D. Ackerman[2]
Physical Ecology Laboratory, University of Northern British Columbia, Prince George, British Columbia V2N 4Z9, Canada

Abstract

Capture of suspended particles by cylindrical collectors is an important mechanism in many aquatic processes, such as larval settlement, suspension feeding, and vegetative filtration. In these processes, the collector Reynolds number (Re_c), based on the collector diameter, ranges from well below 1 to 1,000. No analytical solutions exist to describe capture over most of this range. Capture is typically described by the efficiency, η, defined as the ratio of the upstream span of particles that are captured on the collector to the collector diameter. Here, laboratory experiments are used to measure capture efficiency of a single cylinder as a function of Re_c and particle ratio, R, which is the ratio of particle diameter to collector diameter. Re_c is varied from 50 to 500 and three values of R are used: 0.03, 0.015, and 0.008. The selected particles have a specific gravity of 1.03. For smooth cylinders, capture increases with both Re_c and R but is more strongly dependent on R. This result indicates that, in aquatic systems, where flow velocity and suspended particle type and size are fixed, higher capture efficiency will occur on the smallest collectors (those with largest R). Furthermore, we examine a similar experiment in which particles are collected by branched structures. We show that capture to individual cylindrical branches within a compound structure can be predicted by single-cylinder efficiencies. Finally, capture was increased when roughness elements were added to the collectors.

The capture of suspended particles by submerged structures is important to biological cycles and chemical fates (Raudkivi 1998; Paterson and Black 1999; Elliott 2000). Biologically, suspension feeders utilize hydrosol filtration for food capture (e.g., Rubenstein and Koehl 1977; LaBarbera 1984). In addition, the transport of suspended particles is important in the life cycle of many species. For example, settlement of planktonic larvae is dictated, at least in part, by the physics of particle motion and substrate encounter (e.g., Butman 1987). Further, Eckman (1983) showed that benthic recruitment is strongly dependent on the presence and numerical density of stem structures. Harvey et al. (1995) provided experimental support for hydrodynamic controls on the settlement of bivalve larvae to filamentous branches of benthic algae. Finally, submarine pollination relies on the encounter rate of pollen with individual vegetative elements. Indeed, Ackerman (1995) suggested pollen shape evolved in response to the physics of transport associated with flow around specific plant morphologies.

Chemical fate is often determined by the fate of suspended particles because pollutants such as heavy metals tend to adsorb to suspended particles (Vaithiyanathan et al. 1993; Sansalone and Buchberger 1997). It has long been held that vegetated zones promote particle removal by enhancing residence time (Knight et al. 1999) and reducing resuspension (Lopez and Garcia 1998). Indeed, Gacia et al. (1999) observed that retention of particles by a seagrass meadow is up to 15 times greater than by barren beds. Moreover, some observational studies suggest that capture of particles onto vegetative surfaces is an additional potential mechanism for removing particles (Reay 1972; Stumpf 1983; Jordan et al. 1986; Leonard et al. 1995). For example, Leonard et al. (1995) observed that the capture of sediment on the stems and leaves of *Juncus roemerianus* contributed up to 10% of the total sediment deposition to a tidal marsh. Stumpf (1983) observed that 80% of the suspended material carried by flood waters disappeared within 12 m of the tidal creek and showed that sediment found on the stems of *Spartina alterniflora* accounted for 50% of this loss. Finally, Hosokawa and Horie (1992) observed that, for the same depth and flow speed, the addition of artificial reeds increased particle removal by 38%. These examples suggest that physical filtration by plant structures plays some role in particle removal in aquatic systems. Indeed, the capture of particles by terrestrial plants is already recognized for its impact on air quality (Beckett et al. 1998).

To examine particle capture by submerged elements, we begin with a simple cylindrical collector. A cylindrical geometry approximates a variety of natural collectors such as reed-like wetland vegetation (e.g., *Spartina alterniflora, Phragmites australis*); submerged benthic plants and algae (Harvey et al. 1995); and cilia, bristles, tube-feet and other

[1] Corresponding author (hmnepf@mit.edu).
[2] Present address: Faculty of Environmental Sciences, University of Guelph, Guelph, Ontario N1G 2W1.

Acknowledgements

MRP was funded by the MIT Presidential Fellows Program and NSF Career Award EAR9629259. J.D.A. acknowledges research support from NSERC and the Canada Research Chair Program. T.J.R.P. was funded by the Wallenberg Foundation. The authors thank Dr. Peter Jumars for his helpful and encouraging comments.

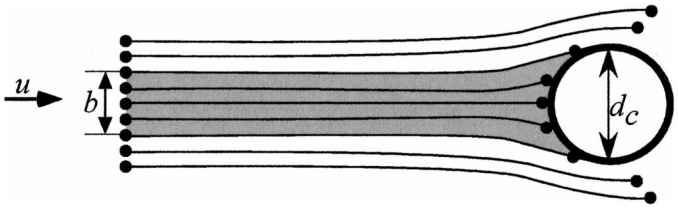

Fig. 1. Definition of capture efficiency. Capture efficiency $\eta = b/d_c$, where b is the width of particles in the flow upstream of the cylinder that will be captured and d_c is cylinder diameter; b is evaluated at an upstream point at which the flow is unaffected by the cylinder.

filamentous structures of suspension feeders (Shimeta and Jumars 1991; Wildish and Kristmanson 1997; Riisgard and Larsen 2001). The relevant length scale for flow around a cylinder is the diameter, d_c, and flow structure is defined by the collector Reynolds number, $Re_c = ud_c/v$, where u is flow velocity and v is kinematic viscosity. In aquatic systems, Re_c typically ranges from well below 1 to 1,000. Collector diameters can range in size from 0.1 mm (a filter element on a suspension feeder; e.g., Shimeta and Jumars 1991) to 2 cm (a large wetland plant stem; e.g., Hotchkiss 1972). Flow velocity u ranges from 0.1 cm s^{-1} to 10 cm s^{-1} and particle sizes reported in the literature range from $d_p = 20$ to 2,000 μm (Shimeta and Jumars 1991). We use these parameters to examine particle capture on smooth and rough cylindrical collectors in a laboratory flume to better understand particle capture in aquatic systems.

Theoretical background

A wealth of literature exists to explain particle capture by a single cylinder at the two limits of creeping and potential flow, defined by $Re_c < 1$ and $Re_c > 1{,}000$, respectively. For a more complete review, please see Rubenstein and Koehl (1977), Spielman (1977), Shimeta and Jumars (1991). However, no analytical solutions exist for the intermediate range $Re_c = 1$–1,000, which is of high interest in aquatic systems.

Capture of particles onto a collector is typically described by the efficiency, η. For a collector of diameter d_c, η is defined as b/d_c, where b is the upstream span of particles that are ultimately captured on the collector. As shown in Fig. 1, η represents the fraction of particles removed from the volume of water passing through the projected area of the collector. Generally, prediction of η considers only how a particle encounters a collector. In this article, we assume that all encounters will lead to particle capture, such that encounter efficiency and capture efficiency are the same. This is a reasonable first-order assumption for aquatic plants and submerged collectors because the sticky periphyton layer (consisting of epiphytes and organic biofilm) that grows on submerged surfaces facilitates particle retention (e.g., Borowitzka and Lethbridge 1989; Guarraci 1999). In our experiments, we use a coating of grease on the cylinder to guarantee that this condition is met.

Particle capture may occur by four primary mechanisms: direct interception, inertial impaction, gravitational deposition, and diffusional deposition (Rubenstein and Koehl 1977; Spielman 1977). Direct interception, η_R, describes capture due to streamline kinematics. If a particle traveling on a streamline approaches a collector within one particle radius, the particle will make contact with the collector and be captured. Equations have been developed to describe this capture at creeping flow ($Re_c < 1$) and potential flow ($Re_c > 1{,}000$). For creeping flow, capture efficiency due to direct interception to a smooth cylinder is

$$\eta_R = \frac{1}{(2 - \ln Re_c)}\left[(1 + R)\ln(1 + R) - \frac{R(2 + R)}{2(1 + R)}\right] \approx \frac{R^2}{(2 - \ln Re_c)} \quad \text{creeping flow} \tag{1}$$

as developed by Langmuir (1942) and Fuchs (1964) based on work by Lamb (1932). Here, R, called the particle ratio, is the ratio of particle diameter, d_p, to collector diameter, d_c. The rightmost portion of the equation is valid for $R < 0.01$. Fuchs (1964) also derived an expression for direct interception to a smooth cylinder based on potential flow

$$\eta_R = 1 + R - \frac{1}{(1 + R)} \approx 2R \quad \text{potential flow} \tag{2}$$

where, again, the simplification at the right-most side of the equation is valid for $R < 0.01$.

Inertial impaction occurs when a particle's inertia causes it to deviate from a streamline and collide with the collector. The influence of a particle's inertia is described by the Stokes number, *Stk*, defined as the ratio of stopping distance, l_s, to cylinder radius. Stopping distance is the additional distance a particle would travel under its own inertia if the fluid were instantly brought to rest. It is a function of particle density, water density, and water viscosity. The Stokes number is thus a function of Re_c, R, and specific gravity s,

$$Stk = \frac{1}{9}Re_c R^2(s - 1) \tag{3}$$

Aerosol theory asserts that there is a critical Stokes number, Stk_{crit}, below which inertial impaction is negligible. For potential flow past a cylinder $Stk_{crit} = 0.125$ (Langmuir and Blodgett 1946; Fuchs 1964). Gravitational deposition occurs when particles settle out of the water column onto surfaces. Diffusional deposition arises from any random process (i.e., Brownian motion, turbulence) that leads particles to deposit on a collector. Natanson (1957) developed the following equation for diffusional deposition efficiency: η_D, for creeping flow,

$$\eta_D = \frac{1.17\pi D^{2/3}}{ud_c}\left[\frac{Re_c v}{2(2 - \ln Re_c)}\right]^{1/3} \quad \text{creeping flow} \tag{4}$$

Particle diffusivity, D, is described by

$$D = (\kappa T)/(3\pi\mu d_p) \tag{5}$$

where κ is the Boltzmann constant, T is absolute temperature, and μ is fluid viscosity (Elimelech et al. 1995).

Capture efficiency, η, defines both the rate at which particles collect on a surface, which is of interest in pollination and suspension feeding, as well as the rate at which particles

are removed from the water column, which is of interest in chemical fate. Consider a cylinder of length l_c. Let P be the number concentration (no. m^{-3}) of particles in the water. Then the flux, F, of particles approaching the cylinder within the region defined by the cylinder's frontal area is

$$F = Pud_c l_c \quad (6)$$

Recall that we define η as the fraction of particles approaching within the frontal area that are ultimately captured. Thus, the rate at which particles are captured on the cylinder (and removed from the water column) is

$$\frac{dN_c}{dt} = \eta Pud_c l_c \quad (7)$$

where N_c is the number of particles captured on the collector over a given duration, t.

Finally, previous capture theories have only considered smooth collectors, e.g., Eq. 1 and Eq. 2 given here. However, aquatic vegetation often grows an epiphytic layer on its submerged surfaces, creating irregularities that may range from micrometers to many millimeters in scale (Borowitzka and Lethbridge 1989; Wetzel 2001). Also, many suspension feeders have roughness or protuberances on their collectors (see review in Wildish and Kristmanson 1997). Roughness elements on a collector surface can affect capture directly, by providing additional surface area, or indirectly, by altering the local flow field. Here we conduct a preliminary assessment of the impact of roughness on capture efficiency by considering both smooth and rough cylinders.

Experimental methods

In this study, we use laboratory experiments to observe the capture of particles by smooth and rough cylindrical surfaces over the range Re_c = 50–500. The total capture efficiency will depend only on Re_c and R because, for the reasons given below, direct interception is the only relevant capture process. First, for specific gravity s = 1.03, the Stokes number ranges from $Stk = 3 \times 10^{-5}$ to 4×10^{-4}, which is significantly smaller than Stk_{crit}, so that the contribution to capture by inertial impaction is negligible. Second, the vertical orientation of the collector precludes gravitational deposition. Finally, while there is no analytical expression for diffusional deposition at Re_c = 50–500, we can estimate η_D for creeping flow from Eq. 4. Because η_D is inversely proportional to u, this estimate is an upper bound for η_D in our experiments. From Eq. 4 and Eq. 5, we find that at $Re_c = 0.1$ and $d_p = 194$ μm, diffusional-deposition efficiency for the particle and collector sizes we use is of order 0.001%. This is an order of magnitude smaller than the capture efficiency we observe, order 0.01% or greater, so we expect that particle capture due to diffusion is negligible in our experiments.

Capture efficiency is measured by allowing particles to collect on a cylinder for duration t. By counting the number of particles collected, N_c, we estimate dN_c/dt and then infer η from Eq. 7. With s = 1.03, P decreased over the duration of the experiments due to settling of particles onto the channel bed. We estimate $P(t)$ by the following expression for the flux of particles to the bed:

$$\frac{dP}{dt} = \frac{-w_s}{h} P \quad (8)$$

where w_s is the settling velocity of the particles (or Stokes' velocity) and h is height of water in the flume. Note that removal due to particle capture provided an insignificant reduction in particle concentration (a typical cylinder collected about 50–200 particles per experiment, far fewer than the millions of particles present in the flume). The decay given in Eq. 8 assumes that turbulence in the water and mixing produced by the pumps keeps the concentration in the water column uniform over depth. This assumption is confirmed by continuous measurements of concentration, which decay exponentially as implied by Eq. 8. The quantity w_s/h is replaced by the constant k, henceforth referred to as the settling rate constant, and Eq. 8 is integrated to derive an expression for concentration decay with time, t,

$$P(t) = P_0 e^{-kt} \quad (9)$$

Incorporating Eq. 9 into Eq. 7 and integrating, we have an expression to estimate capture efficiency that accounts for settling loss,

$$\eta = \frac{N_c k}{P_0 u d_c l_c (1 - e^{-kt})} \quad (10)$$

This equation assumes that capture begins at $t = 0$ and ends at time t. P_0 is the number concentration of particles when the cylinder is inserted. Uncertainty in the experimental capture efficiency was estimated in two ways: (1) propagated uncertainty was calculated for an individual trial (Taylor 1997) and (2) standard error was computed for five replicate trials. However, only the propagated uncertainty is reported, as it was higher than the standard error for every experiment set.

Experiments were conducted in a flume 2.75 m long, 22 cm wide, and 20 cm high. Water depth, h, ranged from 9.0 to 10.5 cm, varying with the Reynolds number desired for each experiment. A recirculating flow was created by up to three different pumps, which included a small centrifugal pump (Micropump, model 101-000) and two peristaltic pumps (Manostat Varistaltic Power Pump model 72-370-000). At the inlet, water was pumped via tubing into a stilling basin and then passed through four aluminum screens (hole diameter 6.35 mm, 57% open area) to straighten the flow (Fig. 2A).

Velocity profiles were measured with an acoustic Doppler velocimeter (ADV, SonTek) and visualized with dye at multiple longitudinal positions. Based on these profiles and the criteria given below, the longitudinal location 2 m downstream of the inlet was chosen for the cylinder test position. We examined the flow in the lateral and vertical directions to determine the thicknesses of the boundary layers and of the central region of uniform flow. At x = 2 m, the lateral profile was not fully developed, with the boundary layers extending <4 cm from each side wall. The middle 14 cm of the flow was laterally uniform. Vertically, the bottom boundary layer extended <4 cm. Above this height, velocity exhibited no more than 10% variation. Thus, we defined a test section of uniform flow between z = 4 cm and the surface. The collector area (see Fig. 2B) was fully inside this

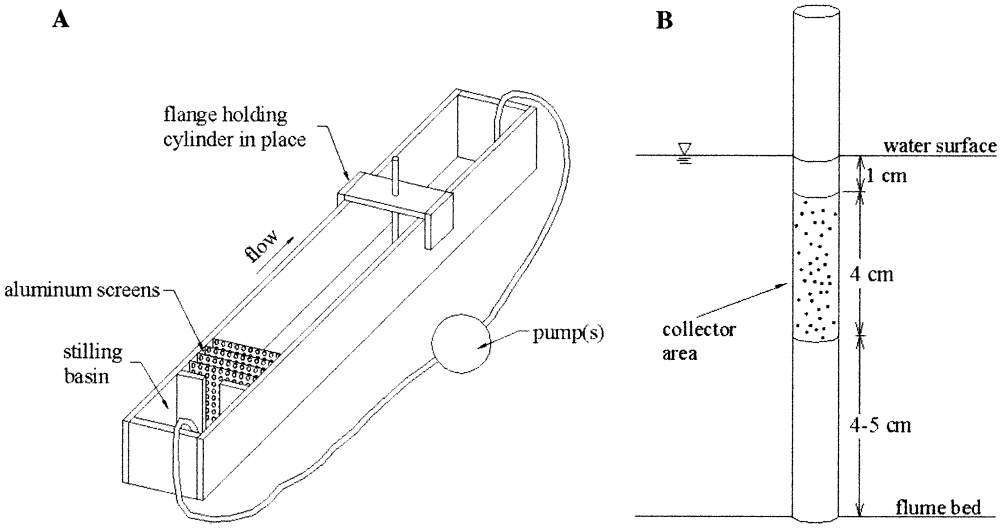

Fig. 2. Flume setup and cylinder dimensions. (A) In the recirculating flume, water is pumped into a stilling basin and then through a set of four aluminum screens that straighten the flow. The cylinder is held in place from above by a flange at a distance of 2 m from the inlet. (B) The collector area on the cylinder is a 4-cm-long section located 1 cm below the surface of the water.

region. The Reynolds number calculated for each trial was based on the average flow velocity from $z = 4$ to $z = h$. Additionally, velocity profiles and dye visualizations indicated that, at a longitudinal position of $x = 2$ m, the suction condition at the outlet did not affect the flow in either lateral or vertical directions.

An industrial plastic resin (Eliokem Pliolite VTAC-L) with specific gravity $s = 1.03$ was chosen for the experimental particles, for its relatively low density, its white color, and its spherical shape. The resin was sieved on a shaker table using U.S. standard sieves #70 and #80, having opening diameters of 210 μm and 177 μm, respectively. The fraction captured between these two sieves was used for the experiments. Assuming a uniform distribution of sizes, the average particle size was 194 μm.

Twelve grams of sieved Pliolite, measured on a scale (Ohaus TS400s, readability 0.01 g), was put into suspension using a small amount of Windex glass cleaner. The suspension was poured into the flume, which was then stirred until the particles spread out over the length of the flume. Because the water recirculated, the same mass of particles could be reused for multiple trials.

Calculation of settling rate—We employed the SonTek ADV to monitor the declining concentration of particles in the flume. An ADV measures velocity by observing the Doppler shift in acoustic waves reflected off particles traveling with the flow. The probe sends out an acoustic pulse at a known frequency and records the change in frequency as the pulse is returned. The strength of the returned signal, measured in decibels, is a function of concentration of particles in the flow. If size and type of particle are uniform, signal strength is directly proportional to the concentration (SonTek 1997). Because decibels are on a logarithmic scale, a difference in signal level is converted to a linear ratio of concentrations by

$$S - S_0 = 10 \log\left(\frac{P}{P_0}\right) \tag{11}$$

where S is the scattering strength in decibels, S_0 is the initial scattering strength in decibels, and (P/P_0) is the ratio of concentration to initial concentration. The factor of 10 in Eq. 11 arises because 1 Bel = 10 dB. Combining with Eq. 9, we get the relation

$$S - S_0 = 10 \log(e^{-kt}) \tag{12}$$

which reduces to a linear equation having the form

$$S = [S_0] - [10k \log(e)]t \tag{13}$$

This linear equation is fitted to observed scattering strength measurements to estimate the settling rate, k.

Scattering strength and particle capture efficiency were not measured simultaneously because the ADV probe tip disrupted the flow. Instead, two replicate concentration records were measured prior to each set of capture experiments. Procedures for taking a concentration record and performing a particle capture trial were identical, the only difference being the presence of the ADV probe tip or the collector cylinder. To ensure that all particles settled out of the flume, each ADV record lasted 40 min, more than four times the average capture experiment (Fig. 3). The sampling rate of each record was 10 Hz.

For each scattering strength record, a linear regression based on 12,000 points gave $r^2 > 0.57$. Standard errors associated with calculating the intercept and slope of the line were always $<1\%$. Based on Eq. 13, the slope m of the linear regression yields the settling rate $k = m/(10 \log(e))$.

Smooth experiments—Three different size Delrin® cylinders of diameters 0.635, 1.27, and 2.54 cm were used as smooth collectors. The manufacturer's tolerance on the Delrin rods is 0.005 cm, and any variation in diameter of the

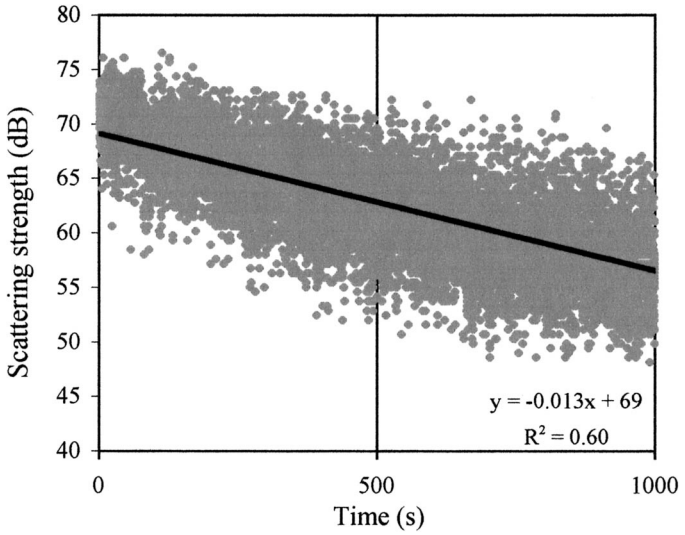

Fig. 3. ADV record of scattering strength versus time taken at 10 s^{-1}. A linear fit (solid line) of the form $S = S_0 - mt$ yields an initial signal level of 69.12 ± 0.06 dB and a settling rate $k = m/[10 \log(e)] = 2.89 \pm 0.02 \times 10^{-3}\ s^{-1}$ (mean ± 95% confidence).

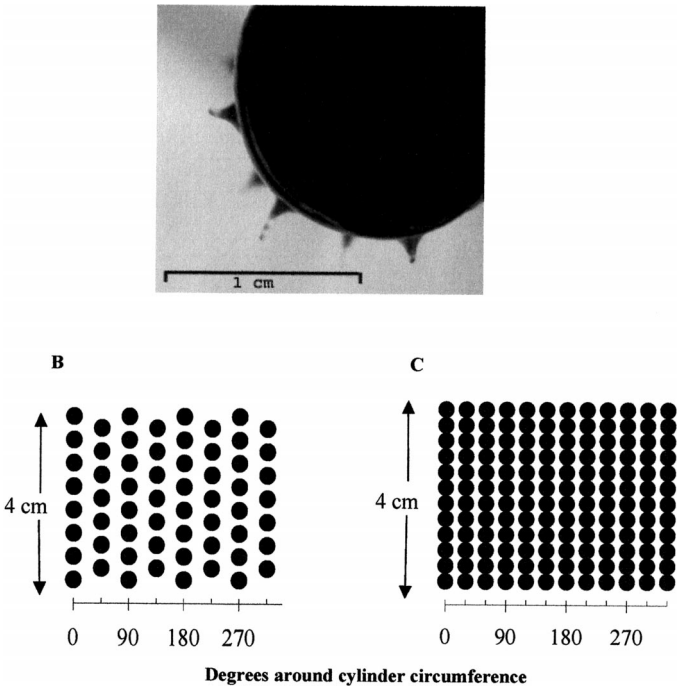

Fig. 4. Geometry and placement of roughness elements. (A) Cross-sectional view of roughness elements. Individual elements had a base diameter of 1.5 mm and protruded 1.5–2 mm. (B) Unrolled arrangement of roughness elements in low-density configuration (4 cm^{-2}). The rows are staggered for a total of 60 elements per cylinder. (C) Unrolled arrangement for high-density configuration (8 cm^{-2}). Here rows are not staggered.

cylinders was negligible. Three different flow rates were used, yielding a total of nine different collector Reynolds numbers, ranging from 50 to 500, and three different R ratios (0.008, 0.016, and 0.03).

Cylinders were prepared by marking off a 4-cm-long test section. In this section, the black Delrin® was left exposed so that the white Pliolite particles would be clearly visible. The rest of the cylinder was covered in white tape. The front of the cylinder, which points directly upstream, was marked with a vertical red line, indicating the zero-degree mark. The cylinder was greased with a liberal coating, about 2–3 mm thick, of clear silicone grease (Chemplex silicone compound 710 by NFO Technologies). The excess was then wiped off with a paper towel in one pass, leaving a thin, uniform coating of negligible thickness ($\ll$1 mm). An end-on visualization confirms that the thickness is uniform around the cylinder and is not thick enough to significantly change the diameter of the cylinder. This process was quite repeatable such that the grease layer thickness was constant from trial to trial.

The flume was stirred by hand for about 1 min until it was fully mixed. Because flow was very turbulent from the mixing, it was allowed to straighten out for 60 s before the cylinder was lowered into the flume. When inserted in the water, the 4-cm test section began 1 cm below the surface of the water so that surface effects were excluded (see cylinder orientation in Fig. 2B). The red line marking zero degrees was aligned with the upstream azimuth. Particles were allowed to collect for a duration ranging from 6 to 10 min, depending on how much time was needed for a substantial number of particles to collect.

The cylinder was removed at the end of the experiment and allowed to dry. It was then photographed with a 4.1-megapixel digital camera (Sony DSC-S85 Cyber-shot®). Although Pliolite particles are visible and could be counted by eye, digital photographs allowed us to magnify the view of the cylinder while collecting photos for future reference. For the smooth experiments, one photo taken from the front was sufficient to photograph almost all the captured particles, because capture was limited to ±50 degrees from the front. During some of the higher Reynolds number experiments, a small number of particles deposited on the back side of the cylinder. These were simply counted by eye, and were usually fewer than 10.

Rough experiments—The procedure for the rough experiments was the same as above, except roughness elements were added during greasing. Instead of roughening the surface of the cylinder and then greasing it, we found that a more uniform and consistent roughness was produced using the grease itself to create roughness elements. These elements retained their shape when inserted into flowing water. A flat nail head was used to apply a dot of grease to the cylinder. The nail head was then pulled away from the cylinder, bringing the grease out to a point and forming a nearly conical-shaped roughness element (Fig. 4A). The diameter at the base of the roughness elements was about 1.5 mm, and the elements protruded 1.5–2 mm. This scale of roughness was chosen because it was significantly larger than the particle size and also larger than the estimated boundary layer thickness on the cylinder. For the 1.27-cm diameter cylinder used for the rough cases, the cylinder boundary layer thickness varied from 0.6 mm to 1.5 mm, depending on the radial position around the cylinder and the Reynolds number (based on numerical calculations, unpublished).

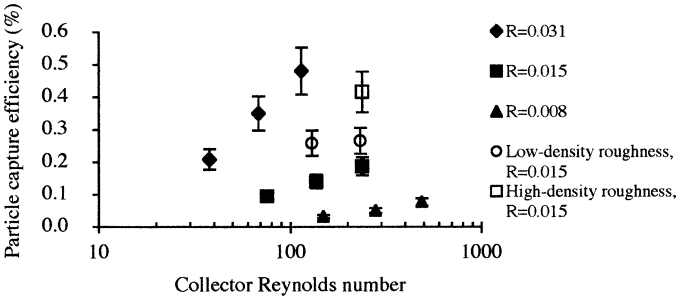

Fig. 5. Capture efficiency versus Reynolds number. Capture efficiency increases with increasing Re_c and R. However, η depends more strongly on R. Cases with roughness show that, for these roughness configurations, η is higher than in the analogous smooth case.

Roughness elements were placed on the cylinder in two array patterns. The low-density configuration consisted of eight staggered rows (a row every 45 degrees) around the cylinder, with a total of 60 elements and a density of about 4 elements cm^{-2} (Fig. 4B). The high-density roughness pattern consisted of 8 elements cm^{-2}. This pattern was made up of 12 rows (a row every 15 degrees) in an unstaggered pattern (Fig. 4C).

With roughness, particle deposition was more spread out than with smooth cylinders, so photographs covered the full 360 degrees of the rough cylinders. During counting, a distinction was made between particles that deposited on a roughness element and those that deposited on a smooth area of the cylinder.

Results

The smooth-cylinder capture efficiency increased with increasing Reynolds number, Re_c, and with increasing particle ratio, R (Fig. 5). However, dependence of η on R is stronger than dependence on Re_c. For example, R must increase by a factor of 1.5 to roughly double the capture, but Re_c must increase by a factor of 3.

Rough experiment sets 10 and 11 were conducted at $Re_c = 240$ and $R = 0.015$, the same values used in smooth experiment set 8. With added low-density roughness (4 cm^{-2}), the capture efficiency increased by 40% (from 0.19% to 0.27%). With high-density roughness (8 cm^{-2}), the capture efficiency increased by 120% (to 0.42%). Experiment set 12 was conducted with low-density roughness at $Re_c = 130$ (comparable with smooth experiment set 2). Capture efficiency again increased with the addition of roughness, now by 85% (from 0.14% to 0.26%).

The spatial distribution of particles also differed between smooth and rough cases. For smooth cylinders, more than 95% of the particles captured deposited on the front 100 degrees of the cylinder. At $Re_c < 200$, no particles were observed to deposit on the back side of the cylinder. At $Re_c > 200$, though, some particles did deposit on the back, but they were fewer than 5% of those captured. This capture is believed to be a consequence of the vortex generation and shedding that occurs behind a cylinder at high Reynolds numbers. Particles on the rough cylinders were more spread out, with significant capture to the roughness elements at the sides of the cylinder. This extended the zone of capture to over 180 degrees of the cylinder's circumference. Similar to the smooth experiments, some capture (<5%) was observed on the back of the cylinder, again presumably due to cylinder wake structures (Table 2).

Table 1. Summary of experimental parameters and results. Twelve sets of experiments were conducted, each with five replicate trials. Collector diameter, d_c, is in cm; Re_c is the collector Reynolds number ($Re_c = ud_c/\nu$); and R is the ratio of particle diameter to cylinder diameter ($R = d_p/d_c$). The error reported is based on the propagated uncertainty for one trial.

Experiment set	Type	d_c (cm)	Re_c	R	Capture efficiency (η) mean (%)
1	Smooth	0.635	68	0.031	0.35±0.05
2	Smooth	1.27	137	0.015	0.14±0.02
3	Smooth	2.54	279	0.008	0.050±0.008
4	Smooth	0.635	38	0.031	0.21±0.03
5	Smooth	1.27	76	0.015	0.094±0.014
6	Smooth	2.54	149	0.008	0.032±0.005
7	Smooth	0.635	115	0.031	0.48±0.07
8	Smooth	1.27	239	0.015	0.19±0.03
9	Smooth	2.54	486	0.008	0.077±0.011
10	Rough-L	1.27	233	0.015	0.27±0.04
11	Rough-H	1.27	239	0.015	0.42±0.06
12	Rough-L	1.27	130	0.015	0.26±0.04

Discussion

Smooth surfaces—As anticipated, neither creeping- nor potential-flow theory is appropriate in the range of $Re_c = 50$–500 considered here (Fig. 6) and representative of conditions in many aquatic systems. However, the observed capture efficiencies fall smoothly between these two theoretical bounds, suggesting that capture efficiency increases monotonically with Re_c.

In any particular aquatic environment, the same flow speed and the same mix of suspended particles are available to all potential collectors. Thus, it is useful to consider how capture efficiency varies across collector size, d_c, given a fixed value

Table 2. Comparison of capture efficiency for smooth, η_{smooth}, and rough cases at corresponding Reynolds number. The total capture to the rough cylinder is η_{rough}; capture to the smooth surfaces of the rough cylinder is $\eta_{rough,SS}$; capture to the roughness elements of the rough cylinder is $\eta_{rough,RS}$, and capture to the front 100 degrees of the rough cylinder is $\eta_{rough,100}$. All efficiencies are in percent (%, mean ± standard error).

Type of capture efficiency	$Re_c = 230$	$Re_c = 130$
η_{smooth}	0.19±0.03	0.14±0.02
η_{rough}	0.27±0.04	0.26±0.04
$\eta_{rough,SS}$	0.13±0.02	0.07±0.01
$\eta_{rough,RS}$	0.13±0.02	0.19±0.03
$\eta_{rough,100}$	0.18±0.03	0.16±0.02

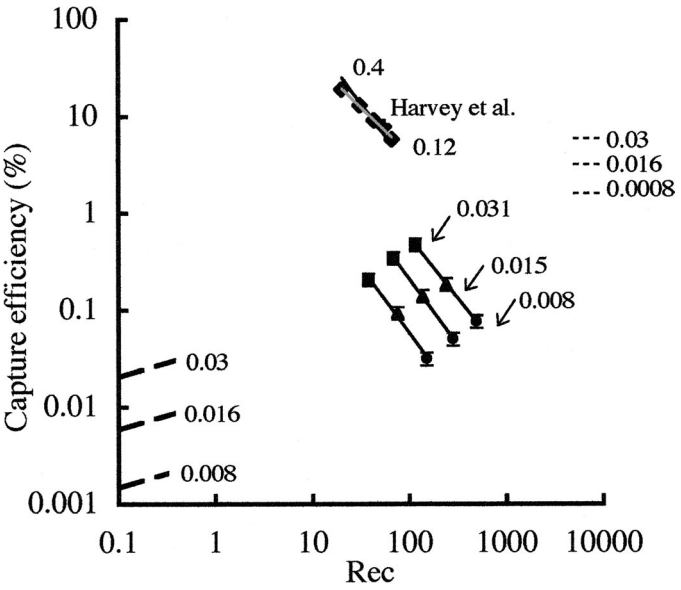

Fig. 6. Observed capture efficiency for smooth cases with three R ratios: 0.031 (solid square), 0.015 (solid triangle), and 0.008 (solid circle). Solid black lines represent power law fits for constant u and varying R, for which we found a constant exponent of 4/3 for the three fits. The creeping flow (thick dashed lines) and potential flow equations (thin dashed lines) do not predict η for Re_c = 1–1,000. Capture efficiencies for a branched structure are taken from Harvey et al. (1995) (solid diamonds). Each data point has a different R, varying from 0.12 to 0.4. Best power-law fit for the Harvey et al. data given as a gray line. For comparison, a 4/3 power law is given in black. Throughout the figure, points and lines are labeled with corresponding R.

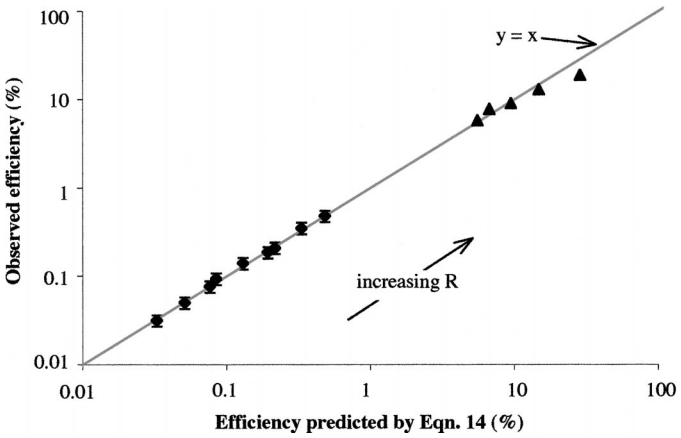

Fig. 7. Comparison of observed capture efficiencies with empirically predicted efficiencies. Observed efficiencies for single-cylinder experiments (black diamonds) are plotted against values predicted by Eq. 14. This empirical relationship also provides good agreement with capture efficiencies on branched structures observed by Harvey et al. (1995) (black triangles).

of u and a fixed set of particle characteristics, or a single characteristic d_p and s. Our observations can be grouped into three series of constant u, as indicated by the lines drawn through our data (Fig. 6). Moving left to right along each line d_c = 0.635 cm, 1.27 cm, and 2.54 cm, respectively, and thus $R = d_p/d_c$ decreases and Re_c increases moving left to right. The smaller diameter collectors capture relatively more particles than the larger diameter collectors, as expressed by higher values of capture efficiency. As a specific example, we compare the rate of capture of a single collector, l_c, of diameter, d_c, to that of two collectors, $2l_c$, of diameter 0.5 d_c. The total capture area is the same for both cases. As described above, η is greater for the smaller diameter collectors, so that from Eq. 7, the total rate of capture, dN_c/dt, will be greater for the pair of smaller diameter collectors.

As discussed earlier, we expect direct interception to be a function of Re_c and R. We looked for an empirical relation of the form $\eta \sim (Re_c)^m(R)^p$. For our nine distinct flow conditions, [Re_c = 50–500 and R = 0.008–0.03], we find that

$$\eta = 0.224(Re_c)^{0.718}(R)^{2.08} \quad (14)$$

fits all experimental data within 10% (Fig. 7). Consistent with existing theory, the exponents on R and Re_c fall between the values found at creeping and potential flow. Keep in mind that Eq. 14 is valid for $Stk < Stk_{crit}$, i.e., direct interception only.

The above trends are also observed by Harvey et al. (1995) for branches of varying diameter within a single structure. Harvey et al. conducted field and laboratory experiments to study the passive accumulation of larvae on epibenthic structures. The larvae of marine benthic invertebrates settle onto epibenthic structures by active and passive accumulation. Active accumulation occurs when larvae chemically or biologically moderate their path, whereas passive accumulation occurs when only hydrodynamic processes control their transport. Harvey et al. investigated the latter case by performing experiments with artificial particles and branch structures. They created filamentous branch structures (Fig. 8), starting with a single branch that bifurcated, with each successive branch bifurcating into branches of progressively smaller length and diameter. Each structure had five branch diameters, ranging from 0.5 to 1.7 mm. Their study used one flow speed of 5 cm s^{-1} and 200 μm-diameter particles of specific gravity s = 1.4. The study reported particles per unit area of branch, mass flow rate of particles, and cylinder geometry. From these parameters, one can es-

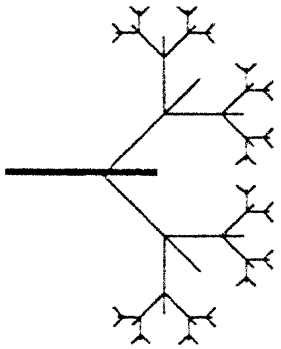

Fig. 8. Branch structure used by Harvey et al. (1995) in flume experiments simulating larval settlement. Multiples of the above two-dimensional structure were assembled to make a three-dimensional branch structure. Branch diameters range from 0.5 to 1.7 mm, with diameter decreasing at each bifurcation.

Table 3. Capture efficiencies computed from data collected by Harvey et al. (1995).

d_c (mm)	Re_c	R	η (%)
0.5	20	0.40	19
0.8	31	0.25	13
1.1	43	0.18	9.1
1.4	55	0.14	7.8
1.7	66	0.12	5.8

timate capture efficiency for each branch diameter (Table 3). Consistent with the single cylinder results reported earlier, the greatest capture efficiency is associated with the smallest branch and decreases monotonically to the largest branch. In addition, Eq. 14 correctly predicts the capture to individual branches within the structure (Fig. 7). This result suggests that Eq. 14 can be used to predict efficiency for collector geometries more complex than single cylinders and for larger R than we examined in this study. However, note that departure from Eq. 14 is expected for very dense structures in which flow interference occurs between branches and particle concentration is diminished for downstream branches.

Particle removal in a typical wetland—As previously discussed, particle capture by vegetation has been indicated as one mechanism by which wetlands reduce suspended particle load (Stumpf 1983; Hosokawa and Horie 1992; Leonard et al. 1995). To quantify the potential importance of this mechanism, we consider a model that accounts for capture to stems as well as gravitational settling in a typical emergent *Spartina alterniflora* coastal wetland. The equation for capture to a single collector, Eq. 7, is rewritten in a per-unit-volume form, where V is volume of water,

$$\frac{1}{V}\frac{dN_c}{dt} = \frac{\eta P u d_c l_c}{V} = \eta P u d_c l_c' \tag{15}$$

N_c/V is equal to P. We define l_c' *as the total collector length per unit volume, or* l_c/V. Additionally, particles may be lost from the water column through settling. We employ a settling model identical to Eq. 8 in which we assume that turbulence keeps the concentration vertically uniform, so that loss due to settling is first order. The total rate of change of suspended particle concentration is then

$$\frac{dP}{dt} = -\eta P u d_c l_c' - \frac{w_s}{h}P \tag{16}$$

We let $K_C = \eta u d_c l_c'$ *and* $K_S = w_s/h$, where K_C and K_S are the rate constants for capture and settling, respectively. After integration, the evolution of concentration in the water column is

$$\frac{P}{P_0} = \exp[-(K_C + K_S)t] \tag{17}$$

To examine the importance of particle capture in a wetland, we compare removal by the combined mechanisms of capture and settling to the removal achieved by settling alone. We define the variable L_{50} as the length of wetland required for the concentration of suspended particles to be reduced by 50%. From Eq. 17,

$$L_{50} = 0.693\left(\frac{u}{K_C + K_S}\right) \tag{18}$$

Table 4. Parameters for wetland removal model. Wetland vegetation was modeled from stand characteristics of short-form and tall-form *Spartina alterniflora* reported by Valiela et al. (1978). d_p, d_c, and u were chosen so that Re_c and R met the requirements of Eq. 14.

	Short form	Tall form
Re_c	6–300	10–1,000
R	0.02–0.6	0.006–0.15
u	1, 5, 10 cm s^{-1}	1, 5, 10 cm s^{-1}
d_p	50, 300 μm	50, 300 μm
d_c	0.5–3 mm	2–9 mm

The physical parameters shown in Table 4 were chosen based on typical values observed in real wetlands (e.g., Valiela et al. 1978), with the constraint that Re_c and R be appropriate for use with Eq. 14. We used two representative particle diameters, 50 and 300 μm, as well as the three flow velocities 1, 5, and 10 cm s^{-1}. Although larger and smaller values of d_p and u might be observed in wetlands, the chosen values give R = 0.006–0.6 and Re_c = 6–1,000, ranges over which Eq. 14 is shown to be valid. Note that we have assumed that the capture efficiency predicted for an isolated cylinder (Eq. 14) can be applied to cylinders within an array, i.e., stems within a canopy. This assumption is valid for sparse canopies in which the interference between stem wakes is weak. Based on wake-interaction studies summarized in White and Nepf (2003), this assumption is expected to be valid for canopy volume fraction less than 5–10%, i.e., for $l_c' d_c^2 < 0.1$.

S. alterniflora has two forms, called short and tall, the primary difference being that stem diameter and height are smaller in the short form. The branches of *S. alterniflora* also contribute to capture. For this calculation, we assume that branch diameter is one half the stem diameter and that submerged branch length is one third of the submerged stem height. We estimated d_c and l_c' using areal stem density, stem height, and histograms of stem diameter as reported by Valiela et al. (1978). For each bin of stem diameters given in the histogram (Valiela et al. 1978), we computed R and Re_c and found η from Eq. 14. We then computed K_C for each bin. The total rate constant is simply the sum over all bins. The canopy volume fraction was calculated as the sum of $l_c' d_c^2$ over all bins. For the short- and tall-forms, respectively, $l_c' d_c^2$ = 0.003 and 0.008, so the sparse canopy assumption is valid. We computed w_s using standard equations for terminal velocity of a settling sphere (see, e.g., Streeter and Wylie 1985). The depth, h, of water in the wetland was taken to be 15 cm, and all the vegetation was assumed to be emergent (i.e., stem height $>$ 15 cm). L_{50} was then calculated from Eq. 18 for particle removal by settling and filtration combined. For comparison, L_{50} contributed by settling alone was calculated from Eq. 18 with $K_c = 0$.

For both particle sizes, removal by particle capture is significant for $u \geq 3$ cm s^{-1} (Fig. 9). Above this flow speed,

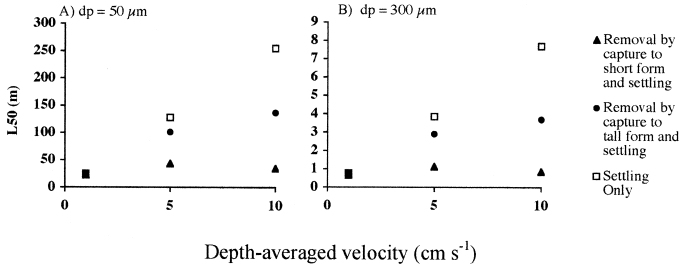

Fig. 9. Particle removal by capture to vegetation and by settling in a typical wetland. L_{50} is the length of wetland necessary to reduce the initial suspended particle concentration by 50%, due either to settling alone (the base case) or to the combination of settling and vegetation capture. Above about $u = 3$ cm s^{-1}, capture to both short- and tall-form *Spartina alterniflora* becomes a significant mechanism of particle removal.

rate of removal due to particle capture is greater by an order of magnitude than the rate of removal due to settling. In general, the decrease in L_{50} is more significant for the short form, reflecting both the higher stem density and smaller stem diameter (higher R) typical of this form. This example indicates that particle capture can contribute significantly to the removal of light particles and pathogens, i.e., with specific gravity 1.03, as considered here.

Rough surfaces—Although this study is not extensive enough to create a complete picture of how particles interact with roughness, some preliminary conclusions can be drawn from our results. For the type and size of roughness used here, particle capture efficiency increases with roughness. However, capture to the front face of the rough cylinder occurs at rates that are nearly identical to the smooth case. Specifically, as shown in Table 2, for the same Reynolds number, the capture to the front 100 degrees of the rough cylinder ($\eta_{\text{rough,100}}$) is nearly the same as the total capture efficiency for the smooth case (η_{smooth}). For $Re_c = 230$, $\eta_{\text{smooth}}/\eta_{\text{rough,100}} = 1.0 \pm 0.1$, and for $Re_c = 130$, $\eta_{\text{smooth}}/\eta_{\text{rough,100}} = 0.87 \pm 0.07$ (mean $\pm$ standard error). The increase in capture from smooth to rough cases is thus the capture that occurs directly to individual roughness elements that protrude into the flow, especially on the sides of the cylinders. That is, the roughness elements function as additional individual collectors. If we take d_{element} to be the average diameter of the conical roughness element, then the particle ratio of the roughness element, R_{element}, is 0.2, which is significantly higher than R for the main collector. Based on η's dependency on R for long cylinders, we qualitatively expect η_{element} to be higher than η observed for the main cylinder. We can estimate η_{element} using the spatial distribution data shown in Table 2, specifically $\eta_{\text{rough,RS}}$ which is the total number of particles that deposited on roughness elements. Dividing $\eta_{\text{rough,RS}}$ by the total number of roughness elements gives an estimate of N_E, the number of particles captured by a single roughness element. From Eq. 7, we can then compute η_{element}. This analysis was only completed for the low-density roughness configuration because spatial distribution data were unavailable for the high-density experiments. For $Re_c = 230$, $\eta_{\text{element}} = 3 \pm 1\%$, and for $Re_c = 130$, $\eta_{\text{element}} = 4 \pm 1\%$ (mean $\pm$ propagated uncertainty). These

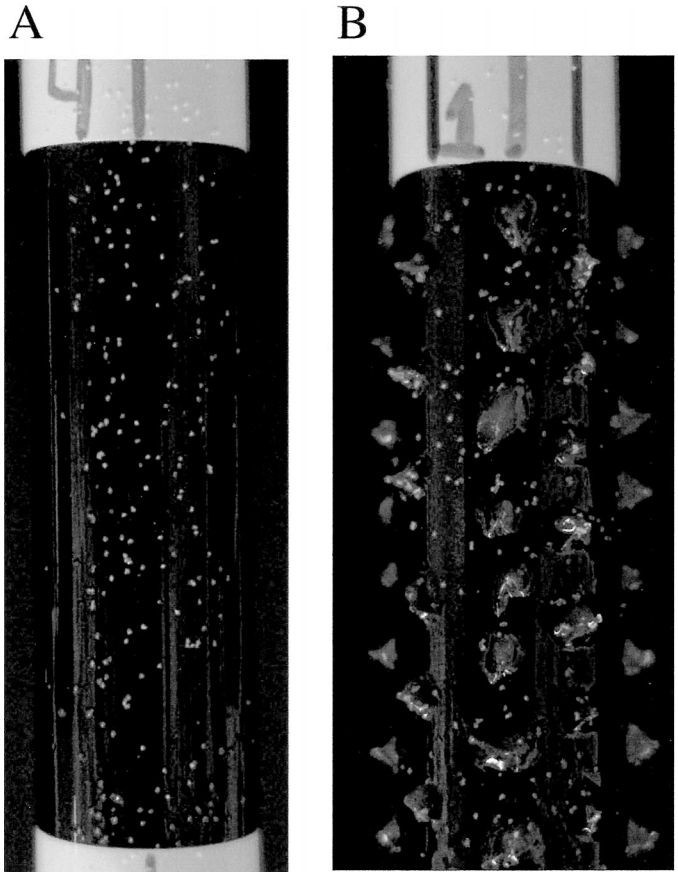

Fig. 10. Sample photos of (A) a smooth cylinder and (B) a cylinder with roughness elements. Except for the addition of roughness, experimental conditions were identical ($Re_c = 230$, $R = 0.015$, $d_c = 1.27$ cm). The rough cylinder's capture efficiency is 40% higher than the smooth cylinder's. Capture on the rough cylinder covers the front 180°, but only the front 100° on the smooth cylinder.

element capture efficiencies are indeed significantly higher than the capture efficiencies of the main cylinder (the highest capture efficiency observed for a main collector was 0.48%). Additionally, we observed dense clusters of particles on the roughness elements (see, e.g., Fig. 10), supporting our belief that they have a high capture efficiency and that the process of capture to them is independent from capture to the large collector. Therefore, it appears that the capture directly to the roughness elements is what augments overall capture to the rough cylinder. However, further studies are needed to more fully describe the impact of roughness on particle capture.

We hypothesize that not all arrangements of roughness will increase capture efficiency. Adding roughness elements to a smooth cylinder increases the cylinder's drag, which in turn pushes the streamlines away from the cylinder boundary. Analogous behavior has been noted in skimming flows over rough beds, where, for sufficiently high density of bed roughness, near-bed flow does not penetrate between the roughness elements but rather skims over the top (Nowell and Church 1979). If flow cannot penetrate the roughness layer on the cylinder surface, then the roughness structures cannot augment particle capture.

To conclude, an empirical power-law function of R and Re_c

is developed to predict particle capture by individual, cylindrically shaped structures at Re_c of 50–500, a range in which both creeping- and potential-flow theory fail. The predicted capture efficiencies are consistent with published values for capture to structures composed of cylindrical branches, indicating that these results can also be applied to more complex shapes. For a limited range of roughness type, the presence of roughness was shown to increase overall capture efficiency.

References

ACKERMAN, J. D. 1995. Convergence of filiform pollen morphologies in seagrasses—functional mechanisms. Evol. Ecol. **9:** 139–153.

BECKETT, K. P., P. H. FREER-SMITH, AND G. TAYLOR. 1998. Urban woodlands: Their role in reducing the effects of particulate pollution. Environ. Pollut. **99:** 347–360.

BOROWITZKA, M. A., AND R. C. LETHBRIDGE. 1989. Seagrass epiphytes, p. 458–498. *In* A. W. D. Larkum, A. J. McComb, and S. A. Shepherd [eds.], Biology of seagrasses. Elsevier.

BUTMAN, C. A. 1987. Larval settlement of soft-sediment invertebrates—the spatial scales of pattern explained by active habitat selection and the emerging role of hydrodynamical processes. Oceanogr. Mar. Biol. **25:** 113–165.

ECKMAN, J. E. 1983. Hydrodynamic processes affecting benthic recruitment. Limnol. Oceanogr. **28:** 241–257.

ELIMELECH, M., J. GREGORY, X. JIA, AND R. A. WILLIAMS. 1995. Particle deposition and aggregation: Measurement, modelling and simulation. Colloid and surface engineering series. Butterworth-Heinemann.

ELLIOTT, A. H. 2000. Settling of fine sediment in a channel with emergent vegetation. J. Hydraulic Eng. **126:** 570–577.

FUCHS, N. A. 1964. The mechanisms of aerosols. Pergamon.

GACIA, E., T. C. GRANATA, AND C. M. DUARTE. 1999. An approach to measurement of particle flux and sediment retention within seagrass (*Posidonia oceanica*) meadows. Aquatic Bot. **65:** 255–268.

GUARRACI, M. 1999. Interaction between epiphyte biomass and resuspended inorganic materials on leaves of natural and artificial submersed vegetation, MS Thesis. Univ. Maryland at College Park.

HARVEY, M., E. BOURGET, AND R. G. INGRAM. 1995. Experimental evidence of passive accumulation of marine bivalve larvae on filamentous epibenthic structures. Limnol. Oceanogr. **40:** 94–104.

HOSOKAWA, Y., AND T. HORIE. 1992. Flow and particulate nutrient removal by wetlands with emergent macrophytes, p. 1271–1282. *In* R. Vollenweider, R. Marchetti and R. Viviani [eds.], Marine coastal eutrophication: Science of the total environment. Elsevier.

HOTCHKISS, N. 1972. Common marsh, underwater & floating-leaved plants of the United States and Canada. Dover.

JORDAN, T., J. PIERCE, AND D. CORRELL. 1986. Flux of particulate matter in the tidal marsh and subtidal shallows of the Rhode River estuary. Estuaries **9:** 310–319.

KNIGHT, R. L., R. H. KADLEC, AND H. M. OHLENDORF. 1999. The use of treatment wetlands for petroleum industry effluents. Environ. Sci. Technol. **33:** 973–980.

LABARBERA, M. 1984. Feeding currents and particle capture mechanisms in suspension feeding animals. Am. Zool. **24:** 71–84.

LAMB, H. 1932. Hydrodynamics, 6th ed. University Press.

LANGMUIR, I. 1942. Filtration of aerosols and the development of filter materials. Report No. 865. Office of Scientific Research and Development.

———, AND K. BLODGETT. 1946. A mathematical investigation of water droplet trajectories. Technical Report No. 5418. U.S. Army Air Force.

LEONARD, L. A., A. C. HINE, AND M. E. LUTHER. 1995. Surficial sediment transport and deposition processes in a Juncus-roemerianus marsh, west-central Florida. J. Coast. Res. **11:** 322–336.

LOPEZ, F., AND M. GARCIA. 1998. Open-channel flow through simulated vegetation: Suspended sediment transport modeling. Water Resour. Res. **34:** 2341–2352.

NATANSON, G. L. 1957. Diffusive deposition of aerosols on a cylinder in a flow in the case of small capture coefficients. Dokl. Akad. Nauk SSSR **112:** 100–103.

NOWELL, A. R. M., AND M. CHURCH. 1979. Turbulent flow in a depth-limited boundry layer. J. Geophys. Res. **84:** 4816–4824.

PATERSON, D. M., AND K. S. BLACK. 1999. Water flow, sediment dynamics and benthic biology. Advances in Ecol. Res. **29:** 155–193.

RAUDKIVI, R. J. 1998. Loose boundary hydraulics, 4th ed. Balkema.

REAY, P. 1972. The accumulation of arsenic from arsenic-rich natural water by aquatic plants. J. Appl. Ecol. **9:** 557–565.

RIISGARD, H. U., AND P. S. LARSEN. 2001. Minireview: Ciliary filter feeding and bio-fluid mechanics—present understanding and unsolved problems. Limnol. Oceanogr. **46:** 882–891.

RUBENSTEIN, D. I., AND M. A. R. KOEHL. 1977. The mechanisms of filter feeding: Some theoretical considerations. American Naturalist **111:** 981–994.

SANSALONE, J. J., AND S. G. BUCHBERGER. 1997. Characterization of solid and metal element distributions in urban highway stormwater. Water Sci. Technol. **36:** 155–160.

SHIMETA, J., AND P. A. JUMARS. 1991. Physical mechanisms and rates of particle capture by suspension feeders. Oceanogr. Mar. Biol. Annu. Rev. **29:** 191–257.

SONTEK. 1997. SonTek doppler current meters—using signal strength data to monitor suspended sediment concentration. SonTek.

SPIELMAN, L. A. 1977. Particle capture from low-speed laminar flows. Am. Rev. Fluid Mech. **9:** 297–319.

STREETER, V., AND E. B. WYLIE. 1985. Fluid mechanics, 8th ed. McGraw-Hill.

STUMPF, R. P. 1983. The process of sedimentation on the surface of a salt marsh. Estuarine, Coastal and Shelf Sc. **17:** 495–508.

TAYLOR, J. R. 1997. An introduction to error analysis: The study of uncertainties in physical measurements. Univ. Science Books.

VAITHIYANATHAN, P., A. RAMANATHAN, AND V. SUBRAMANIAN. 1993. Transport and distribution of heavy-metals in Cauvery River. Water Air Soil Pollut. **71:** 13–28.

VALIELA, I., J. M. TEAL, AND W. G. DEUSER. 1978. The nature of growth forms in the salt marsh grass *Spartina alterniflora*. Am. Nat. **112:** 461–470.

WETZEL, R. G. 2001. Limnology, lake and river ecosystems, 3rd ed. Academic.

WHITE, B., AND H. NEPF. 2003. Scalar transport in random cylinder arrays at moderate Reynolds number. J. Fluid Mech. **487:** 43–79.

WILDISH, D., AND D. KRISTMANSON. 1997. Benthic suspension feeders and flow. University Press.

Received: 1 May 2003
Accepted: 30 July 2003
Amended: 11 August 2003